Int. J. Electrochem. Sci., 17 **(2022)** Article Number: 221237, doi: 10.20964/2022.12.42

International Journal of
ELECTROCHEMICAL
SCIENCE
www.electrochemsci.org

Short Communication

Facile Synthesis of Walnut-like Haggite by One Step Hydrothermal Method

Yan Xue[1,*], *Lu Fang*[1], *Qing-Qing Zhou*[2], *Qian-Wen Li*[2], *Lin Chen*[1], *Junjun Zhang*[1]

[1] School of Physics and Materials Engineering, Hefei Normal University, Hefei 230601, P. R. China
[2] College of Light Textile Engineering and Art, Anhui Agricultural University, Hefei 230036, P. R. China
[*]E-mail: xueyan@mail.ustc.edu.com

Received: 22 September 2022 / *Accepted:* 7 November 2022 / *Published:* 30 November 2022

After seventy years of unsuccessful attempts, Haggite $V_4O_6(OH)_4$ micro/nanostructures have been first synthesized successfully for the first time in this study via a one-step facile hydrothermal method using polymer polyvinyl pyrrolidone (PVP, K30) as a capping reagent. XRD, XPS, and SEM were used to study the structure, composition and morphology of the walnut-like $V_4O_6(OH)_4$. The synthetic sample exhibits a hierarchical morphology of a novel walnut-like microarchitecture assembled by single crystalline nanosheets. The PVP content and the pH have been demonstrated to play key roles in the formation of walnut-like $V_4O_6(OH)_4$ in the hydrothermal system. This synthesis of stable $V_4O_6(OH)_4$ by a hydrothermal method with a layered structure provides a novel method for synthesizing vanadium oxyhydroxides, and the good cycle stability of $V_4O_6(OH)_4$ has been confirmed the potential application to aqueous lithium-ion cells.

Keywords: Haggite, Walnut-like, One Step, Hydrothermal, Aqueous lithium ion cell

1. INTRODUCTION

Various vanadium oxyhydroxides have exhibit numerous structures with different compositions and valences. These materials have been used in various applications, such as cathode materials for rechargeable Li-ion batteries[1], sodium-ion battery anodes[2], catalysts for oxidation reactions[3-4], electrocatalysts for urea oxidation[5], electrodes for Zn-ion batteries[6], supercapacitor electrodes[7-8], and smart electrical switch materials[9]. Therefore, an increasing number of vanadium oxyhydroxides have been developed by various synthetic methods. Although new phase hollandite-type VOOH quadrangular nanorods have been developed by hydrothermal method as a novel smart material[10], but the controllable synthesis of vanadium oxyhydroxides remains challenging. Controlled synthesis of middle-valent vanadium oxyhydroxides containing V^{3+} and V^{4+} is widely known to be very difficulty.

However, the vanadium oxyhydroxides have a particularly rich variety of structural motifs of middle valence states, including both V^{3+} and V^{4+}. There are at least ten known V^{4+} oxides, further hindering precise control of the synthesis of V^{4+} oxyhydroxides.

Haggite is a well known V^{4+} oxyhydroxides and a scarce black vanadium mineral, that was discovered in the 1950s in the Colorado Plateaus. At that time, the chemical formula of haggite was first elaborated as $V_2O_2(OH)_3$ by Evans and Mrose[11]. Due to the lack of chemical synthesis methods, all the chemical and physical properties of haggite were determined from mineral samples until a study performed by Wu et al[12]. Haggite was first successfully obtained by a two-step synthetic method, using $V(OH)_2NH_2$ as a precursor and formic acid as an oxidizer, and the formula was finally carefully elucidated as $V_4O_6(OH)_4$, and haggite was found to exhibit with semiconductor-insulator transitions. Subsequently, Besnardiere et al. synthesized of haggite by an aqueous method in the presence of hydrazine over a long period of 4-5 days[13]. Later on, $V_4O_6(OH)_4$ was prepared by the reduction of poisonous vanadium(V) pentoxide in a mixture of guaiacol and methanol, where guaiacol was used to prevent the over reduction of haggite to V_2O_3[14]. In summary, the development and application of haggite has been limited by synthetic methods based on complex steps, long reaction times, poisonous reactants and organic solvents. Therefore, developing a facile, safe and convenient way to synthesize stable haggite is found to be very important for realizing large-scale practical application.

Numerous vanadium oxyhydroxides have been researched as potential battery materials due to the variety of morphological and atomic structural configurations exhibited by these compounds. [1-2,6-8] Haggite is a typical semiconductor with a band gap of 1.4eV and consists of double octahedron chains that form the corrugated sheets parallel to the (001) plane (Figure 1a and 1b). Besides, the typical layered structure inspired us that the special structure is favoured to the de/intercalation of ion. Similar to many vanadium oxyhydroxides, haggite exhibits unique electrochemical properties upon ion insertion but suffers from poor cycling stability[12]. To prevent this detrimental effect, smart formulations for haggite are urgently needed.

Herein, the haggite walnut-like micro/nanostructures were successfully synthesizedby a simple one-step template-free hydrothermal route at low temperature for the first time using HCl as a pH regulator and facilitated by the coordination effect of PVP. This method for the synthesis of walnut-like haggite micro/nanostructures in the absence of the vacuum conditions was demonstrated to be useful, economical, and effective for industrial production. In addition, we introduced a walnut-like micro/nanostructure as an active material into aqueous lithium-ion batteries for the first time. As expected, the electrode based on walnut-like haggite exhibited enhanced electrochemical properties and cycle retention resulting from a unique 3D framework, rigid morphology and characteristic layered structure.

2. EXPERIMENTAL

2.1. Materials

Analytical grade of hydrochloric acid and ethanol were purchased from Shanghai Chemical Reagents Co. and used without further purification. Sodium orthovanadate ($Na_3VO_4 \cdot 12H_2O$), oxalic acid

($H_2C_2O_4·2H_2O$), polymer polyvinyl pyrrolidone (PVP), Cetyltrimethylammonium bromide (CTAB), and sodium hexadecyl sulfate (SDS) were purchased from Alfa Aesar.

2.2. Synthesis of Haggite

A beaker was successively filled with 6 mmol (2.4 g) of $Na_3VO_4·12H_2O$, 10 mmol (1.26 g) of $H_2C_2O_4·2H_2O$ and 30 mL of distilled water, and the mixture was stirred gently for approximately 10 min to produce a transparent yellow solution. Next, 9 mL of a 2 M HCl solution were added slowly dropwise into the solution under stirring. The solution changed from yellow to orange and finally to a clear dark green. Then, a prescribed quantity of PVP (0.02 g, 0.05 g, etc.) was added to the dark green solution under vigorous stirring for 30 min. The resulting homogeneous solution was sealed in a 50-mL autoclave and heated at 180 ℃ for 24 h. The system was cooled to room temperature, and the final product was collected by centrifugation by washing with deionized water and ethanol several times to remove potential ionic residues and then dried in vacuum at 60 ℃.

2.3. Characterization

The obtained samples were characterized by X-ray powder diffraction (XRD) with Cu Kα radiation (λ=1.54178 Å). X-ray photoelectron spectroscopy (XPS) measurements was performed on a VGESCALAB MKII X-ray photoelectron spectrometer. Field emission scanning electron microscopy (FESEM) images were taken on a JEOL JSM-6700F SEM. Transmission electron microscopy (TEM) images were carried out on a JEOL-2010 TEM.

2.4. Electrochemical Measurements

The electrochemical properties of the $V_4O_6(OH)_4$ hierarchical walnut-like structures for aqueous lithium-ion batteries were investigated using prepared model test cells. Negative and positive electrodes was similarly prepared. Test electrodes were fabricated by mixing the as-prepared $V_4O_6(OH)_4$ samples (80 wt %), acetylene black (10 wt %), and polyvinylidene fluoride (PVDF) (10 wt %). The electrolyte was an aqueous solution of 5 M $LiNO_3$ and 0.001 M LiOH. Discharge and charge tests were carried out on aqueous lithium-ion batteries using a Land battery system (CT2001A) at a constant current density of 60 mA h g^{-1} with a cut-off voltage of 1.5-0.5 V

3. RESULTS AND DISCUSSION

The synthetic $V_4O_6(OH)_4$ was prepared by a simple one-step template-free hydrothermal route, which an aqueous solution of Na_3VO_4 and $H_2C_2O_4$ was reacted with PVP as a capping reagent at pH ~2 for 24 h at 180 ºC. The typical XRD pattern of $V_4O_6(OH)_4$ product was showed in Figure 1c. All the strong and sharp diffraction peaks could be perfectly indexed to the monoclinic $V_4O_6(OH)_4$ (JCPDS 74-

1688), and its lattice constants were a=12.17Å, b=2.99Å, c=4.83Å, and β=98.25° (space group: C2/m), indicating the high purity of the product. Besides, XPS analysis revealed the further information on the chemical composition and valence state of the synthesized samples. The survey spectrum in Figure 1f revealed that the average atomic ratio of V and O in the as-prepared product is 1:2.52 based on the quantification of V 2p and O 1s peaks. The obtained binding energies of the product were corrected by referencing C 1s to 284.50 eV. In Figure 1f, the binding energies of the V 2p peaks showed at ca. 516.3 and ca. 523.9 eV respectively, which corresponded to V(IV) according to the previous results[12]. The asymmetry in the right part of High resolution XPS (HRXPS) for O1s region (Figure 1g) indicated a contribution from more than one oxygen. Actually, the core level centred at 530.06 eV, 531.28 eV, and 531.98 eV can be assigned to the O^{2-} in the V-O, O-H and the small amounts of physically absorbed H_2O respectively, which was in good agreement the structural information in haggite structure[9]. Notably, signals for hydrogen atoms could not be detected in the XPS spectrum. The very small N 1s peak in Figure 1e was assigned to the PVP, not completely removed by simple washing[14]. Therefore, the as-obtained sample was confirmed as pure monoclinic haggite according to the results of XRD and XPS results.

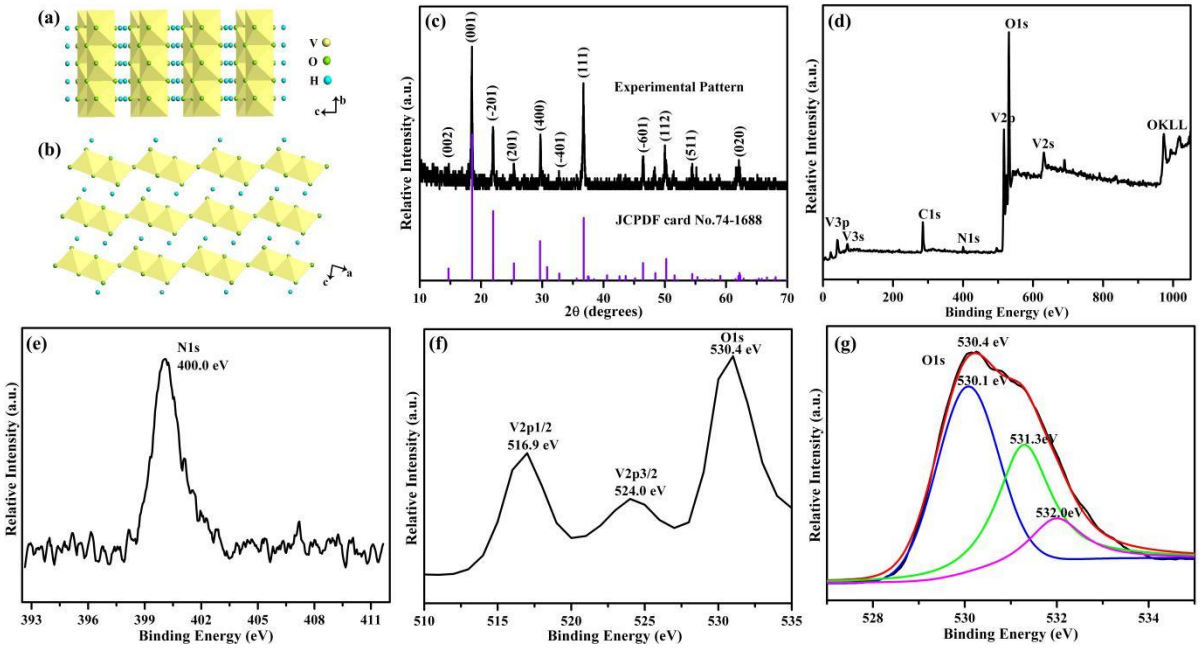

Figure 1. (a) Packing diagrams of crystal structure projected along [001] and (b) [010]; (c) XRD pattern; (d) full XPS spectrum; (e) HRXPS for N1s region; (f) core-level spectra of V 2p and O 1s; (g) HRXPS for O 1s region.

Figure 2 represented FESEM images showing large-scale Haggite $V_4O_6(OH)_4$ hierarchical micro/nanostructures. In Figure 2a, the SEM image showed typical product with uniform, walnut-like moicroarchitecture ~3-5 μm in diameter. Then, the more detailed morphology of the walnut-like micro/nanostructure with intact smooth surface was showed in the Figure 2b. Significantly, the 3D walnut structures were formed through connections between nanoplates. These nanoplates were ca. 100-

200 nm thick, as evidenced by the erect spindle fringe in the SEM images (Figure 2b). More interestingly, a lot of different pores were composed of nanoplates in the spindle micro/nanostructure, which may served as transport channels for ions or small molecules, as showed in Figure 2b.

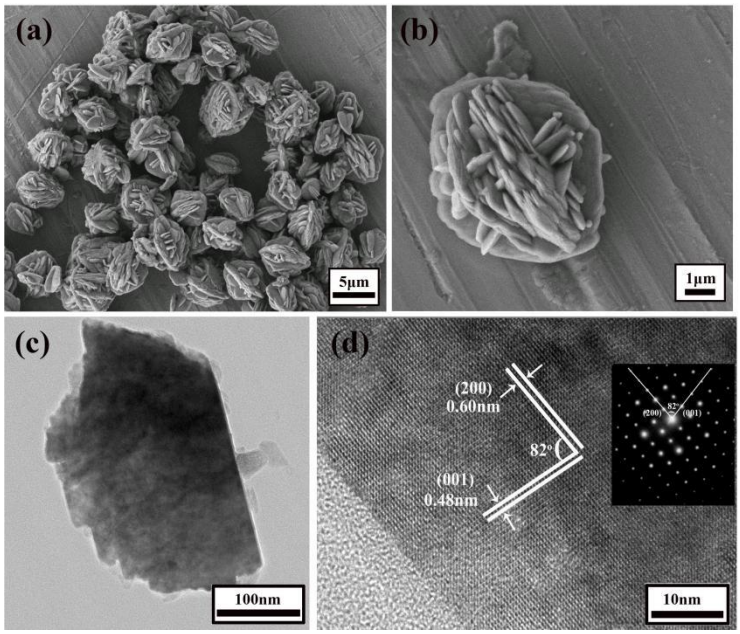

Figure 2. Representative FESEM images of haggite $V_4O_6(OH)_4$ microstructures, (a) overall morphology, (b) individual structure; (c) TEM image of a nanoplate from walnut like $V_4O_6(OH)_4$ microstructures; (d) HRTEM image of the edge of $V_4O_6(OH)_4$ nanoplate (inset: corresponding SAED pattern an individual nanosheet).

More information about obtained $V_4O_6(OH)_4$ was showed from the TEM images. $V_4O_6(OH)_4$ nanoplates had diameters of ca. 400 nm in Figure 2c, which agreed well with the SEM images of Figure 2a. The representative HRTEM image and SAED pattern inset in Figure 2d clearly showed the crystalline structure of a nanoplate of the synthetic haggite $V_4O_6(OH)_4$ micro/nanostructures. The interplanar distances of 4.77 Å and 6.04 Å match well with the d_{001} and d_{200} spacing of the haggite $V_4O_6(OH)_4$, respectively. Additionally, the orientation angle value of (001) and (200) is found to be 82°. The clear lattice fringes and bright ED show the good crystallinity of the synthetic haggite $V_4O_6(OH)_4$.

It is well known that the Haggite $V_4O_6(OH)_4$ crystal structure was constituted by two different types of connections between VO_6 octahedra, as shown in Figure 1b. In our case, the hydrolyzation of Na_3VO_4 was restored by $H_2C_2O_4$, leading to the formation of the coordinated cation $[VO(H_2O)_6]^{2+}$. In addition, as schematized in Figure 3, the coordination of the O of PVP to vanadium, served as a binding site for metal ions and hindered further condensation of the vanadium complex at two chelating positions. Then, in the presence of the PVP, subsequent condensation of the $[VO(H_2O)_6]^{2+}$ complex occurred by vertex- or edge-sharing for VO_6 octahedra(Figure 3), which was similar to the condensation of ferric ions[15]. As one might expect, the VO_6 octahedra with either vertex- sharing or edge- sharing produced the final crystal structure of $V_4O_6(OH)_4$. The similar formation process has also been found for the synthesis of VO_2(B) hierarchical flower-like structures in the presence of PVP [14].

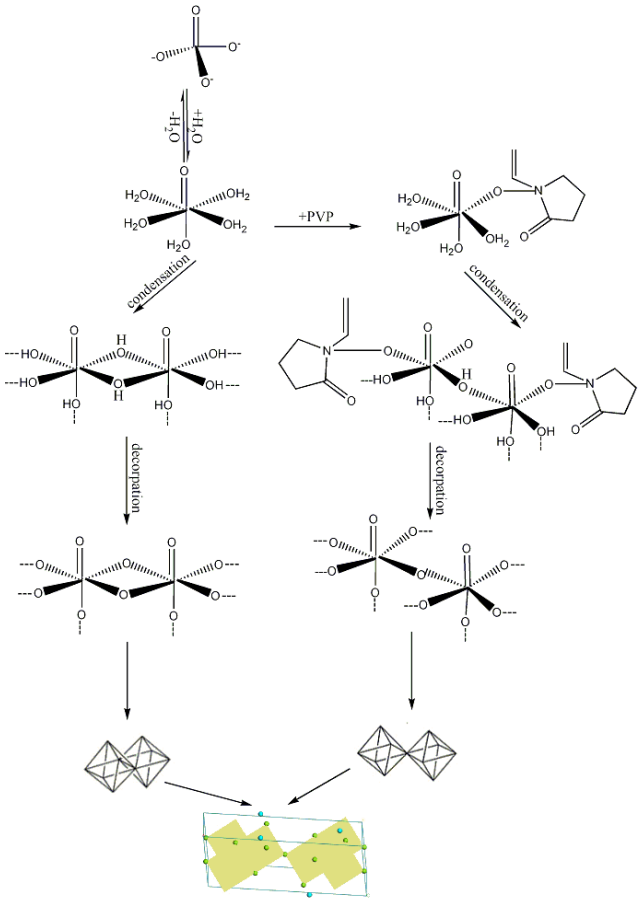

Figure 3. Schematic illustration for the formation of $V_4O_6(OH)_4$.

As is well known, the existing form of the V in the solution is sensitive to the acidity of the entire hydrothermal system. Therefore, to study the effect of the acid concentration, different volumes of a 2 M HCl solution and different weights of $H_2C_2O_4$ were added to the reaction system(Figure 4). As showed in the Figure 4a, the volume of the 2 M HCl less than 9 mL, the obtained product is VO_2(B) rather than $V_4O_6(OH)_4$ micro/nanostructures. As showed in the Figure 4b, the weight of $H_2C_2O_4$ less than 10 mmol, the obtained product is VO_2(B) rather than $V_4O_6(OH)_4$ micro/nanostructures. The obtained product is influenced by the the acidity of the whole hydrothermal system. In fact, the similar phenomenon is often found in the molybdate system as well[16].

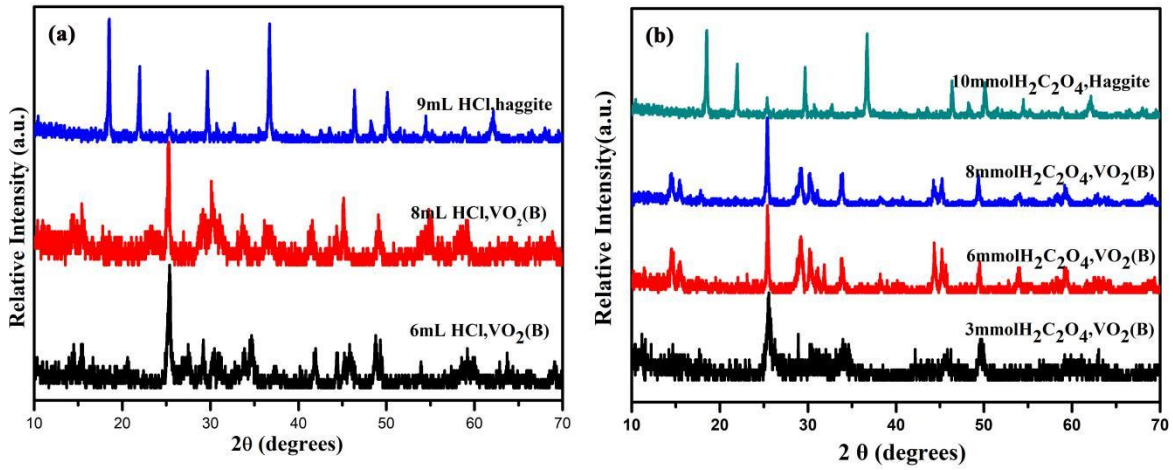

Figure 4. the product in the system with different acid concentration.

The surfactant PVP was one of the most commonly used crystal growth modifiers for inorganic structures. To investigate the effect of PVP on the formation of the walnut-like hierarchical structure of $V_4O_6(OH)_4$, comparative experiments without PVP were carried out. Surprisingly, the product could not be obtained in the system without PVP. That is, the presence of the polymer PVP is the essential factor for the formation of the $V_4O_6(OH)_4$. Similar effects of the presence of PVP have been reported for the formation of the novel phases of VO_2(D) and InOOH.[17-18]

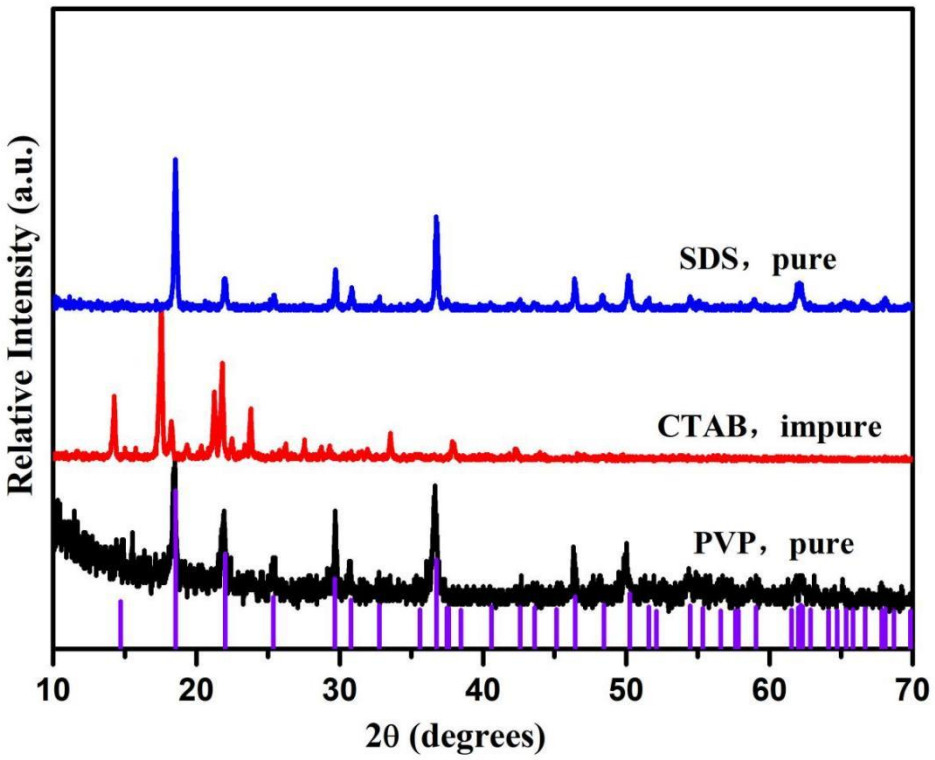

Figure 5. the product in the system with and without different surfantants.

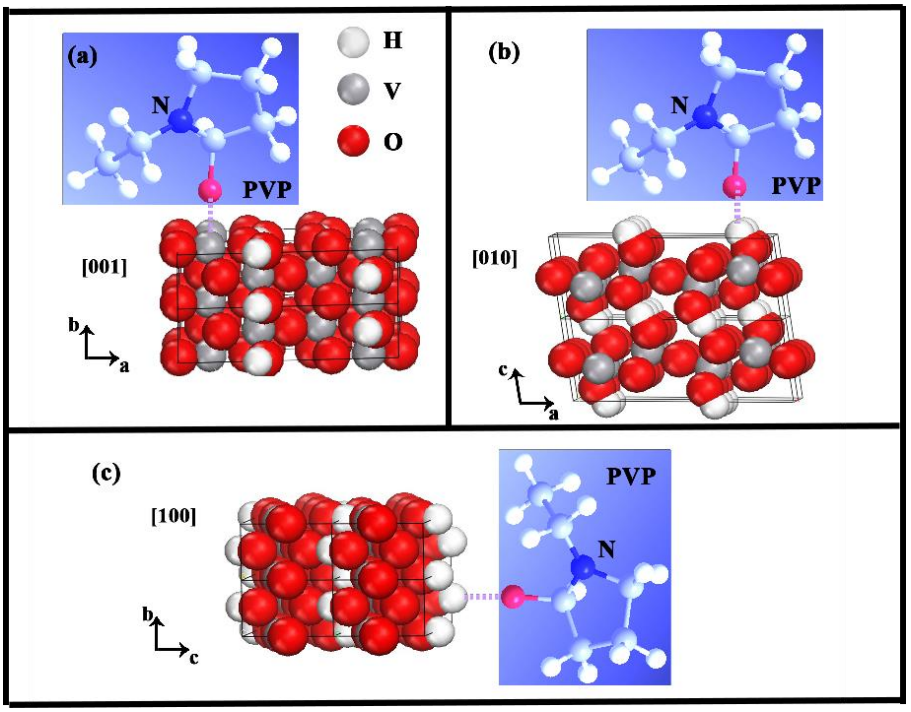

Figure 6. The schemtic of (a) V in the [010] coordinate with O in PVP, (b) and (c) H in the [001] coordinate with O in PVP.

Although the detailed effect of PVP in the formation of $V_4O_6(OH)_4$ remains unclear, it is reasonable to speculate that PVP absorbs on the H in the [001] of $V_4O_6(OH)_4$ (Figure 6b and Figure 6c) and coordinates with V in the [010](Figure 6a), stabilizing the $V_4O_6(OH)_4$ in the solution. It is well known that $V_4O_6(OH)_4$ and VO_2(B) have similar crystal structures. These structures differ in that the H in the [001] direction creates a subtle change in the crystal structure of haggite $V_4O_6(OH)_4$. To further elucidate the coordination effect of the O in the PVP, CTAB and SDS were used to replace PVP in the hydrothermal process as capping agents. As expected, the $V_4O_6(OH)_4$ formed successfully in the hydrothermal system by stabilization of the H in the [001] direction through coordination bonding of O in SDS (Figure 5). By contrast, $V_4O_6(OH)_4$ did not form in the presence of CTAB in the hydrothermal system (Figure 5). In brief, the coordination effect of the PVP plays a key role in the formation of the $V_4O_6(OH)_4$. The similar formation process has been observed for VO_2(B) hierarchical structures built from nanoplates in the presence of PVP[14]. The interaction between PVP and $V_4O_6(OH)_4$ crystals was confirmed by the XPS results shown in Figure 1d. The very small N 1s peak (Figure 1e) in the XPS data was indicated the presence of the few PVP. Because PVP was absorbed on the surface of the obtained product and required several rinses of distilled water and ethanol to be completely washed off.

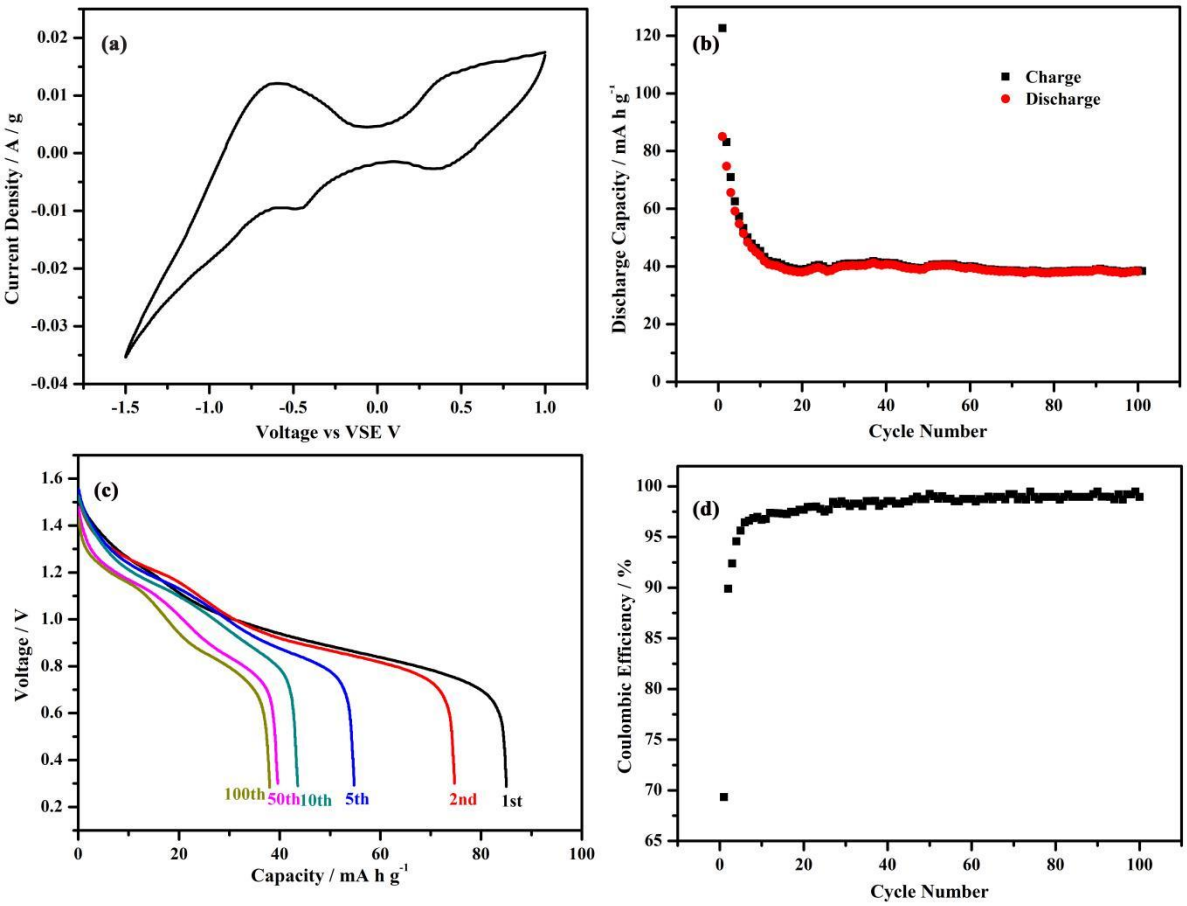

Figure 7. (a) Cyclic voltammograms at 50 mV s^{-1}, (b) and (d) cycling stability at 60 mA g^{-1}, (c) Voltage versus discharge capacity curves for the $V_4O_6(OH)_4$/$LiMn_2O_4$ cell between 1.5 and 0.2 V at the 1st, 2nd, 5th, 10th, 50th and 100th cycle in aqueous electrolyte.

In general, structure determines material properties. The unique microscopic structure and macroscopic features make synthetic walnut-like $V_4O_6(OH)_4$ a potential material for aqueous lithium-ion cells. The layered structure of $V_4O_6(OH)_4$ could facilitate Li^+ diffusion. The unique walnut-like morphological features increase the interfacial area between the electrode and electrolyte and decrease the diffusion distance for lithium ions, both of which were key factors for optimizing the performance of an aqueous lithium-ion cell. In fact, Haggite has useful electrochemical properties but suffers from poor cycling stability[12]. To prevent this detrimental effect, smart formulations for haggite are urgently needed. Based on these considerations, we introduced $V_4O_6(OH)_4$ as an active material into water-based lithium-ion batteries for the first time, where an aqueous electrolyte solution is safer and less expensive than currently used electrolytes[19].

Table 1. Cycling properties of vanadium oxyhydroxides under different test conditions reported by different research groups.

Battery system	Current density [mA cm^{-2} or mA g^{-1}]	Discharge capacity [mA h g^{-1}] / cycle	Capacity retention [%] / cycles	Ref.
walnut-like $V_4O_6(OH)_4/LiMn_2O_4$ aqueous cell	60	85/1, 39.8/50, 38.2/100	46.8/50, 42.5/100	this work
Groove-like L-VOOH /$LiMn_2O_4$ aqueous cell	60	113.6/1, 36.2/50	31.9/50	1
hollow spheres VOOH /$LiMn_2O_4$ aqueous cells	60	61.4/1, 21.4/50	34.9/50	1
LiV_3O_8/$LiCoO_2$ aqueous cells	0.2	55/1	36/100	21
haggite-based Li cell (nonaqueous cells)		230/1, 100/50	43/50	12
hollow nanourchins VOOH/$LiMn_2O_4$ aqueous cell	60	72.1/1, 28.2/50	39/50	22
VOOH nanorods/$LiMn_2O_4$ aqueous cell	60	43.5/1, 13.2/50	30/50	22

The cyclic voltammograms, charge/discharge curves and corresponding cycle behaviours of $V_4O_6(OH)_4/LiMn_2O_4$ at voltages of 1.5 and 0.2 V and a current density of 60 mA h g^{-1} are shown in Figure 7. This figure shows that it is possible to extract Li ions from the host before the evolution of O_2. The results for $V_4O_6(OH)_4$ show two pairs of reduction peaks at -0.6656 and -0.07762V (the reduction potential vs. SCE) and oxidation peaks at -0.606 and 0.3787V, corresponding to the insertion/extraction of Li ions into the $V_4O_6(OH)_4$ before H_2 evolution. seen that using the electrode based on the haggite $V_4O_6(OH)_4$ walnut-like micro/nanostructure results in an average voltage for the $V_4O_6(OH)_4/LiMn_2O_4$ cell of approximately 0.9 V (with a range between 0.8 and 1.0 V), which is similar to those of Ni-MH and Ni-Cd rechargeable systems (ca. 1.2 V). This voltage is similar to that of primary Zn-MnO_2 batteries, making the $V_4O_6(OH)_4$-based aqueous lithium-ion batteries (ALIB) excellent alternatives to Zn-MnO_2 batteries. Table 1 shows the cycling properties of vanadium oxyhydroxides under different test conditions reported by different research groups. The highest discharge capacity of the $V_4O_6(OH)_4/LiMn_2O_4$ aqueous cell is 85 mA h g^{-1}, which is higher than that of a reported ALIB system[1, 20-22], making our aqueous lithium-ion battery a promising substitute for cells. The discharge capacity of the $V_4O_6(OH)_4/LiMn_2O_4$ aqueous cell is 39.8 mA h g^{-1} and 38.2 mA h g^{-1} at the 50th and 100th cycles, respectively. This discharge capacity is higher than that of a groove-like L-VOOH/$LiMn_2O_4$ aqueous cell (36.2 mA h g^{-1} at the 50th cycle). [1] The capacity retention of the walnut-like $V_4O_6(OH)_4/LiMn_2O_4$ aqueous cell is 46.8% and 42.5% after 50 cycles and 100 cycles, respectively, which is also higher than that of a hollow-urchin-like VOOH/$LiMn_2O_4$ aqueous cell (39% after 50 cycles) and haggite-based Li cells (43% after 50 cycles). [12,22] In addition, the coulombic efficiency increases gradually and

saturates after several cycles, indicating that the electrochemical system has achieved equilibrium. The overall average coulombic efficiency is approximately 98% for the haggite electrode for our aqueous cells, indicating good reversibility during long-term charge/discharge tests. These results lead to the conclusion that the walnut-like haggite electrode obtained by a one-step hydrothermal method has enhanced electrochemical properties and cycle retention.

4. CONCLUSION

In summary, a novel walnut-like hierarchical $V_4O_6(OH)_4$ micro/nanostructure was successfully synthesized for the first time through a one-step solution method using PVP as a capping reagent. This one-step method results in a simple and controllable synthesis. The absorbance of O by PVP and acidity play key roles in the formation of haggite ($V_4O_6(OH)_4$), providing a novel way to synthesize novel vanadium oxyhydroxides. The highest discharge capacity of the walnut-like $V_4O_6(OH)_4/LiMn_2O_4$ aqueous cell has a maximum discharge capacity of 85 mA h g^{-1} and a capacity retention of 46.8% and 42.5% after 50 and 100 cycles, respectively. A characteristic layered structure and unique walnut-like hierarchical micro/nanostructure make $V_4O_6(OH)_4$ a potential anode electrode material.

ACKNOWLEDGEMENTS
This work was supported by the grant from the National Natural Science Foundation of China (21501040), and the Key Project of Natural Science Research in Anhui Colleges (KJ2021A0132), National College Student Innovation Training Program (202110364055), the Hefei Normal University High-Level Talent Research Startup Fund (2020rcjj11), the Key Research Project of Hefei Normal University(2021KJZD22, 2021KJZD24).

References

1. H. Zhu, S. C. Ruan, *Mater. Lett.*, 184(2016) 134.
2. W. B. Li, J. F. Huang, L. L. Feng, L. Y. Cao, Y. Q. Feng, H. J. Wang, J. Y. Li, C. Y. Yao, *J. Mater. Chem. A*, 5(2017) 20217.
3. Y. Cui, Y. Xue, R. Zhang, J. Zhang, X. A. Li, X. B. Zhu, *J. Mater. Chem. A*, 7(2019) 21911.
4. L. Yan, X. W. Chen, X. J. Liu, L. P. Chen, B. Zhang, *J. Mater. Chem. A*, 8(2020) 23637.
5. D. D. Wei, W. J. Tang, N. N. Ma, Y. L. Wang, *Mater. Lett.*, 291(2021) 129593.
6. J. J. He, X. Q. Liu, H. Z. Zhang, Z. J. Yang, X. Shi, Q. Y. Liu, X. H. Lu, *ChemSusChem*, 13(2020) 1568.
7. M. Chen, Y. F. Zhang, J. Q. Zheng, Y. Y. Liu, Z. M. Gao, Z. H. Yu, C. G. Meng, *Mater. Lett.*, 227(2018) 217.
8. C. Xu, M. Li, K. B. Li, Z. Y. Du, J. W. Chen, F. X. Zou, S. C. Xu, N. Li, G. H. Li, *J. Alloys Compd.*, 869(2009) 159367.
9. C. Z. Wu, J. Dai, X. Zhang, J. L. Yang, Y. Xie, *J. Am. Chem. Soc.*, 131(2009) 7218.
10. C. Z. Wu, X. Yie, L. Y. Lei, S. Q. Hu, C. Z. Ou Yang, *Adv. Mater.*, 18(2006) 1727.
11. H. T. Evans, M. E. Mrose, *Acta Crystallogr.*, 11(1958) 56.
12. J. Besnardiere, X. Petrissans, F. Ribot, V. Briois, C. Surcin, M. Morcrette, V. Buissette, T. Le Mercier, S. Cassaignon, D. Portehault, *Inorg. Chem.*, 55(2016) 11502.
13. F. Yan, Y. Bai, Y. Sang, L. Yu, K. Wu, K. Cui, Z. Wen, F. Mai, Z. Ma, H. Chen, Y. Li, *Inorg. Chem.*, 57(2018) 8705.

14. S. Zhang, Y. Li, C. Wu, F. Zheng, Y. Xie, *J. Phys. Chem. C.*, 113(2009) 15058.
15. Z. C. Wu, M. Zhang, K. Yu, S. D. Zhang, Y. Xie, *Chem. Eur. J.*, 14(2008) 5346.
16. M. B. Rammal, S. Omanovic, *Molecules*, 27(2022) 776.
17. L. Liu, F. Cao, T. Yao, Y. Xu, M. Zhou, B. C. Pan, S. Wei, Y. Xie, *New J. Chem.*, 36(2012) 619.
18. T. T. Tseng, W. J. Tseng, *Ceram. Int.*, 35(2009) 2837.
19. D. Bin, Y. Wen, Y. Wang, Y. Xia, *J. Energy Chem.*, 27(2018) 1521.
20. W. Li, J.R. Pahn, D.S. Wainwright, *Science*, 264(1994) 1115.
21. G.J. Wang, L.J. Fu, N.H. Zhao, et al. *Angew. Chem. Int. Ed.*, 46(2007) 295.
22. Y. Xu, L. Zheng, Y. Xie, *Dalton Trans.*, 39(2010) 10729.